Resonant terahertz reflection of periodic arrays of subwavelength metallic rectangles

Xinchao Lu,[1] Jiaguang Han,[1,2] and Weili Zhang[1,a)]
[1]*School of Electrical and Computer Engineering, Oklahoma State University, Stillwater, Oklahoma 74078, USA*
[2]*Department of Physics, National University of Singapore, 2 Science Drive 3, Singapore 117542, Singapore*

(Received 5 February 2008; accepted 5 March 2008; published online 25 March 2008)

We present reflection properties of terahertz pulses in periodic arrays of metallic rectangles of subwavelength dimensions. Resonant reflection is characterized by terahertz time-domain spectroscopy and is attributed to the contributions from the dipole localized surface plasmons of isolated metallic rectangles, their interactions between the rectangles, and the nonresonant direct reflection. A number of factors, including the polarization of the terahertz electric field, the shape of the metal structures, the dielectric function of the substrate, and the lattice constant of the arrays are found to influence terahertz reflection properties. The measured resonant reflectance is well fit by numerical simulations. © *2008 American Institute of Physics*. [DOI: 10.1063/1.2902292]

Subwavelength metallic structures have been extensively studied in developing terahertz components, such as photoconductive transmission lines, waveguides, polarizers, filters, photonic crystals, and plasmonic crystals. Of particular interest, two-dimensional arrays of subwavelength holes patterned on metallic films, as referred to as plasmonic crystals, have demonstrated enhanced terahertz transmission, primarily due to resonant excitation of surface plasmons at the metal-dielectric interface.[1–7] It shows promising applications in terahertz generation, detection, spectroscopy, subwavelength imaging, and biosensing.

In contrast to the holes, when an electromagnetic wave is incident upon the surface of isolated subwavelength metallic particles, resonant reflection may occur due to excitation of dipolar localized surface plasmons (DLSPs).[8,9] Under the influence of electric field, metallic particles can be polarized and dipoles are induced as a result, leading to DLSPs. The field enhancement due to DLSPs has led to unique plasmonic optical antennas.[10] In the visible frequency regime, resonant excitation of DLSPs in nanoparticles, characterized by extinction spectroscopy, plays an important role in surface enhanced Raman scattering, biosensors, and optoelectronic devices.[11–15]

At terahertz frequencies, due to drastic increase in the value of complex permittivity, most metals become highly conductive. The plasmonic structures could reveal unique properties as compared to those at visible frequencies.[3–7,16] In this letter, we investigate terahertz properties of periodic arrays of subwavelength metallic rectangles by terahertz time-domain spectroscopy (TDS) reflection measurements.[17] Resonant terahertz reflection is observed and is influenced by the polarization of the terahertz electric field, the shape of the subwavelength structures, the dielectric function of the substrate, and the lattice constant of the rectangles. Terahertz reflection properties are analyzed by the Fano model and the CST MICROWAVE STUDIO simulations. The characteristic reflection is found to be associated with both resonant and nonresonant contributions.

Square arrays of subwavelength structures made from 190 nm thick aluminum films are processed by photolithography and metallization on substrates of either silicon (0.64 mm thick, *n*-type resistivity $\rho=12\ \Omega\ \mathrm{cm}$) or fused quartz (1.03 mm thick). Resonant properties of the arrays are measured by use of a photoconductive switch-based terahertz TDS spectrometer configured in a reflection geometry under normal incidence. The array sample, with dimensions of $25\times25\ \mathrm{mm}^2$, is positioned at the $1/e$ amplitude terahertz beam waist with radius of 8 mm at 0.5 THz to ensure optimum beam quality at the array surface.[18] An unpatterned 190 nm thick Al film processed on identical substrates is used as the reference in the terahertz TDS characterization. The absolute amplitude reflection is defined as $|\tilde{r}(\omega)|=|E_s(\omega)|/|E_r(\omega)|$, where $E_s(\omega)$ and $E_r(\omega)$ are the Fourier-transformed frequency-dependent amplitudes of the terahertz pulses reflected by the array and the reference, respectively.

The measured terahertz pulses reflected by an array of $80\times100\ \mu\mathrm{m}^2$ Al rectangles on silicon and the reference are illustrated in Fig. 1(a). In the terahertz TDS characterization, the *P*-polarized terahertz electric field is parallel to the longer axis (y) of the rectangles, $E\|y$, as shown in the inset of Fig. 1(a). The lattice constant of the array is 160 μm in both x and y directions, giving the filling fraction of metal as 31.25%. Figure 1(b) shows the frequency-dependent reflectance extracted through the relation $R(\omega)=|\tilde{r}(\omega)|^2$ from the Fourier-transformed terahertz pulses. The corresponding phase change is plotted in the inset of Fig. 1(b). A peak reflectance $R_p=0.90$ is observed at 0.52 THz and this well-defined maximum can be attributed to both resonant and nonresonant reflections. The resonant reflection is associated with DLSPs of isolated metal rectangles and the interactions of DLSPs between the adjacent rectangles, while the nonresonant contributions are comprised of direct reflections by the rectangles and the substrate.

The resonance frequency due to DLSPs excited at a single subwavelength rectangle can be approximately described by $\omega_r/2\pi=(c/2L)\varepsilon_d^{-1/2}$, where L is the length of the rectangles parallel to the polarization of the incident electric field, ε_d is the dielectric constant of the substrate, here $\varepsilon_d=11.68$ for silicon; the contribution of the imaginary

a)Electronic mail: wwzhang@okstate.edu.

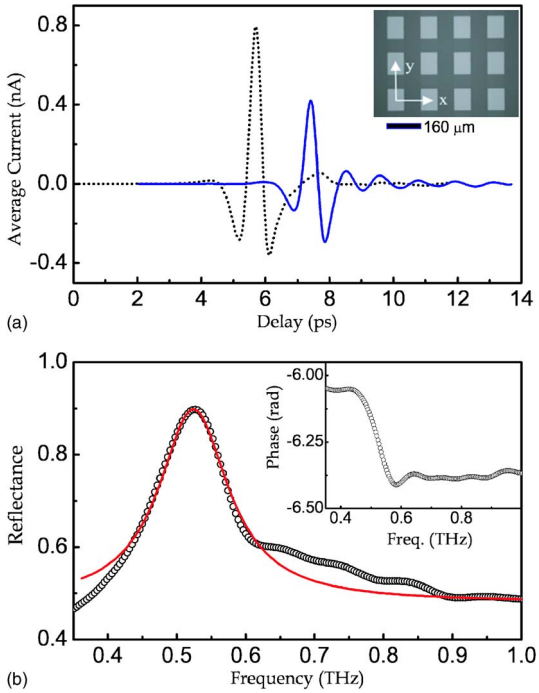

FIG. 1. (Color online) (a) Measured terahertz pulses reflected by the 80 μm (x axis) $\times$100 μm (y axis) rectangle array patterned on silicon (lattice constant 160 μm and $E\|y$, solid curve) and the reference (dotted curve), respectively. For clarity, the sample terahertz pulse is horizontally shifted by 2 ps. Inset: microscopic image of the array. (b) Frequency-dependent reflectance. Measured data: open circles and Fano fit: solid curve. Inset: corresponding phase change. The parameters used in the Fano fit are $\omega_\nu/2\pi$=0.524 THz, $\Gamma_\nu/2\pi$=0.14 THz, R_a=0.48, R_b=4.65$\times10^{-6}$, and q_ν=300.

dielectric constant of the lightly doped silicon can be negligible.[19] Thus, the calculated resonance frequency of the single 80$\times$100 μm^2 metal rectangle on silicon is 0.44 THz, which is lower than the measured reflection peak 0.52 THz of the periodic array; the latter, as mentioned above, is a result of both resonant and nonresonant contributions.

The Fano model is employed to analyze the reflection properties,[20–24] in which the reflection lineshape of the plasmonic structures is considered as a result of two scattering processes: the discrete resonant state and the continuum direct scattering state. The Fano reflection probability R is defined as $R_{\mathrm{Fano}}=|\tilde{r}(\omega)|^2=R_a+R_b(1+\Sigma_\nu q_\nu/\varepsilon_\nu)^2/[1+(\Sigma_\nu 1/\varepsilon_\nu)^2]$, which specifies the coupling between the discrete and the continuum states. For an isolated resonance, the Fano model can be written as $R_{\mathrm{Fano}}(\omega)=R_a+R_b(\varepsilon_\nu+q_\nu)^2/(1+\varepsilon_\nu^2)$, where $\varepsilon_\nu=(\omega-\omega_\nu)/(\Gamma_\nu/2)$, R_a is a slowly varying reflectance, $|R_b|$ is a coefficient describing the contribution of the zero-order continuum state coupled to the discrete resonant state, $\omega_\nu/2\pi$=0.524 THz and $\Gamma_\nu/2\pi$=0.14 THz are the peak frequency and the linewidth of the resonant state, respectively, and q_ν is the Breit–Wigner–Fano coupling coefficient. As shown in Fig. 1(b), the Fano model enables a consistent fit to the measured reflectance of the asymmetric lineshape.

Reflection properties of the array patterned on both silicon and quartz substrates are compared. As shown in Fig. 2(a), a giant frequency shift of 0.30 THz is observed in the measured peak reflectance for rectangles of dimensions 40 $\times$80 μm^2 as the boarding medium is changed from silicon to quartz. This result is considerably consistent with the dependence of resonance frequency on the dielectric function of substrate, $\omega_r/2\pi\propto\varepsilon_d^{-1/2}$, here ε_d=3.82 for fused quartz.

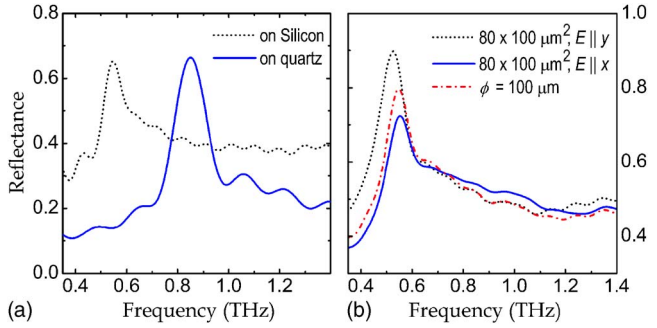

FIG. 2. (Color online) (a) Measured frequency-dependent reflectance of the Al rectangles with dimensions of 40 μm (x axis) $\times$80 μm (y axis) and a lattice constant 160 μm on silicon and quartz substrates with terahertz electric field $E\|y$. (b) Comparison of measured reflectance of the 80 $\times$100 μm rectangles with different polarizations of incident terahertz field and the circular structures of a diameter Φ=100 μm. These metal structures are patterned on silicon with the same lattice constant 160 μm.

No clear difference is seen in the peak reflectance; however, the background reflectance shown at nonresonant frequencies with the quartz substrate is significantly reduced. This is mainly due to the lower dielectric constant of quartz than that of silicon, giving rise to a reduced background reflection by the nonmetal sites of the array.

In Fig. 2(b), we show the dependence of resonant reflection on polarization of incident terahertz electric field. With the 80 μm (x axis)$\times$100 μm (y axis) rectangles, both the resonance frequency and the reflectance exhibit polarization dependent behavior. The resonance frequency shifts from 0.55 to 0.52 THz as the terahertz polarization is switched from $E\|x$ to $E\|y$, while the peak reflectance is enhanced from 0.72 to 0.90. This can be explained when the terahertz pulses are incident upon the array, the polarized electric field induces opposite signs of charges at the ends of the isolated rectangle along the polarization of electric field. As such, the charge oscillation gives rise to DLSPs.[25] When the dimension of the rectangle along the electric field increases, the separation between the intraparticle charge oscillations is increased as well. It thus degrades the force between the intraparticle charges and consequently lets to a redshift in peak reflection. Meanwhile, the increased separation between the intraparticle charges results in a higher dipole moment, leading to an enhanced reflectance with $E\|y$.

To explore shape dependent reflection properties, a square array of circular structures with a diameter of 100 μm is patterned on silicon, while the other parameters remain the same as those of the 80$\times$100 μm^2 rectangles. As shown in Fig. 2(b), both the resonance frequency and peak reflectance of the circular structures sit right between those of the rectangles of two different orientations, due to shape dependent intraparticle charge distributions. This result indicates that the resonant reflection of subwavelength structures of similar filling fractions indeed exhibits shape dependent behavior.

The effect of lattice constant of metal rectangles on resonant reflection is also characterized. A set of square arrays of 100$\times$80 μm^2 rectangles with various lattice constants are processed on silicon substrates. When the lattice constant varies from 160 to 280 μm^2, as shown in Fig. 3, both the measured peak reflectance and resonance frequency exhibit a characteristic evolution. The peak reflectance decreases with increasing lattice constant due to reduced density of rectangles, as well as the degraded interactions between DLSPs of the adjacent rectangles. This lattice-constant dependent

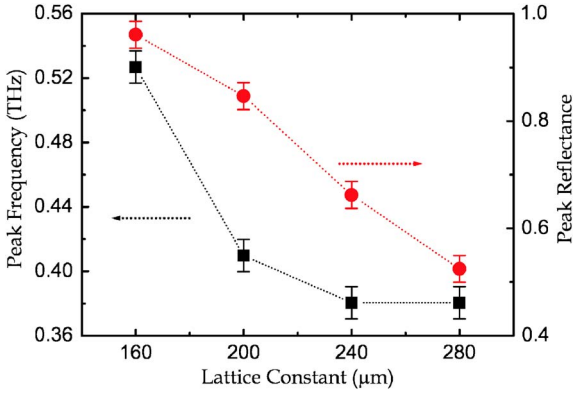

FIG. 3. (Color online) Dependence of resonant frequencies and peak reflectance on lattice constant. The arrays are patterned on silicon. The lattice constants are 160, 200, 240, and 280 μm, respectively. The dimensions of the rectangles are 80 μm (x axis) $\times$100 μm (y axis) with $E\|y$.

resonance shift is primarily due to interactions between DLSPs of the adjacent rectangles and can be explained in terms of long-range electrodynamic interaction.[9] When the lattice constant is on the order of one half of the wavelength of incident electromagnetic waves, the retardation between the rectangles causes the induced dipole fields out of phase, leading to a redshifted resonance with increasing lattice constant.[10,26] However, when the lattice constant is beyond 240 μm, the resonance frequency does not show further shift because the interactions between DLSPs of the adjacent rectangles become negligible. The observed characteristic resonance shift agrees well with the simple semianalytical model for the infinite array of particles.[9]

CST MICROWAVE STUDIO (CST Studio Suite 2006B, NUS) simulations are carried out to model the Al arrays of subwavelength rectangles. The solid curve in Fig. 4(a) shows a simulated resonant reflectance of the 80×100 μm^2 rectangles with a 160 μm lattice constant and $E\|y$. It shows a good agreement with the experimental data and captures

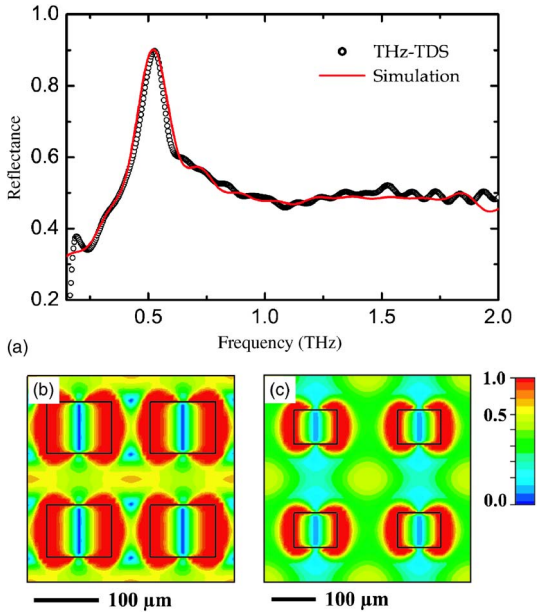

FIG. 4. (Color online) (a) Measured (open circles) and CST MICROWAVE STUDIO simulated (solid curve) frequency-dependent reflectance of the 80 μm (x axis) $\times$100 μm (y axis) Al rectangles patterned on silicon with a lattice constant of 160 μm and $E\|y$. (b) and (c) Simulated electric field distributions in the arrays of different lattice constants: (b) 160 μm and (c) 240 μm.

most of the observed behavior, such as the resonance frequency, amplitude, and lineshape. The simulated reflectance linewidth, however, appears slightly broader due to possible experimental variations in the Al thin-film conductivity and patterned structures.[27] Figures 4(b) and 4(c) illustrate the simulated electric field distributions of the arrays with two different lattice constants, 160 and 240 μm, respectively. In Fig. 4(b), electric field coupling is clearly revealed at the gaps along the incident terahertz electric filed due to interactions of DLSPs between the adjacent rectangles. When the lattice constant is increased from 160 to 240 μm, however, this interaction is extensively degraded, as shown in Fig. 4(c), confirming the contributions of DLSP interactions to the observed lattice-constant dependent characteristic reflection presented in Fig. 3.[9] Resonant reflection properties of these plasmonic structures are promising in integrated plasmonic terahertz devices, subwavelength terahertz spectroscopy, and terahertz biomedical sensing.

The authors acknowledge stimulating discussions with S. Zhang. This work is partially supported by the National Science Foundation.

[1] T. W. Ebbesen, H. J. Lezec, H. F. Ghaemi, T. Thio, and P. A. Wolff, Nature (London) **391**, 667 (1998).
[2] R. Gordon, M. Hughes, B. Leathem, K. L. Kavanagh, and A. G. Brolo, Nano Lett. **5**, 1243 (2005).
[3] D. Qu, D. Grischkowsky, and W. Zhang, Opt. Lett. **29**, 896 (2004).
[4] G. Torosyan, C. Rau, B. Pradarutti, and R. Beigang, Appl. Phys. Lett. **85**, 3372 (2004).
[5] J. Saxler, J. G. Rivas, C. Janke, H. P. M. Pellemans, P. H. Bolver, and H. Kurz, Phys. Rev. B **69**, 155427 (2004).
[6] J. W. Lee, M. A. Seo, D. J. Park, D. S. Kim, S. C. Jeoung, C. Lienau, Q. H. Park, and P. C. M. Planken, Opt. Express **14**, 1253 (2006).
[7] J. B. Masson and G. Gallot, Phys. Rev. B **73**, 121401 (2006).
[8] U. Kreibig and L. Genzel, Surf. Sci. **156**, 678 (1985).
[9] C. L. Haynes, A. D. Mcfarland, L. Zhao, R. P. Van Duyne, and G. C. Schatz, J. Phys. Chem. B **107**, 7337 (2003).
[10] E. J. Smythe, E. Cubukcu, and F. Capasso, Opt. Express **15**, 7439 (2007).
[11] K. H. Su, Q. H. Wei, and X. Zhang, Nano Lett. **3**, 1087 (2003).
[12] N. Felidj, J. Aubard, G. Levi, J. R. Krenn, M. Salerno, G. Schider, B. Lamprecht, A. Leitner, and F. R. Aussenegg, Phys. Rev. B **65**, 075419 (2002).
[13] A. Hartschuh, E. J. Sanchez, X. S. Xie, and L. Novotny, Phys. Rev. Lett. **90**, 095503 (2003).
[14] Y. Cao, R. Jin, and C. A. Mirkin, Science **297**, 1536 (2002).
[15] S. A. Maier, P. G. Kik, and H. A. Atwater, Appl. Phys. Lett. **81**, 1714 (2002).
[16] A. K. Azad, Y. Zhao, W. Zhang, and M. He, Opt. Lett. **31**, 2637 (2006).
[17] D. Grischkowsky, S. Keiding, M. Van Exter, and Ch. Fattinger, J. Opt. Soc. Am. B **7**, 2006 (1990).
[18] W. Zhang, J. Zhang, and D. Grischkowsky, Appl. Phys. Lett. **78**, 2425 (2001).
[19] K. B. Crozier, A. Sundaramurthy, G. S. Kino, and C. F. Quate, J. Appl. Phys. **94**, 4632 (2003).
[20] U. Fano, Phys. Rev. **124**, 1866 (1961).
[21] C. Genet, M. P. Van Exter, and J. P. Woerdman, Opt. Commun. **225**, 331 (2003).
[22] W. Fan, S. Zhang, B. Minhas, K. J. Malloy, and S. R. J. Brueck, Phys. Rev. Lett. **94**, 033902 (2005).
[23] J. Han, A. K. Azad, M. Gong, X. Lu, and W. Zhang, Appl. Phys. Lett. **91**, 071122 (2007).
[24] W. Zhang, A. K. Azad, J. Han, J. Xu, J. Chen, and X.-C. Zhang, Phys. Rev. Lett. **98**, 183901 (2007).
[25] J. Aizpurua, G. W. Bryant, L. J. Richter, and F. J. García de Abajo, Phys. Rev. B **71**, 235420 (2005).
[26] B. Lamprecht, G. Schider, R. T. Lechner, H. Ditlbacher, J. R. Krenn, A. Leitner, and F. R. Aussenegg, Phys. Rev. Lett. **84**, 4721 (2000).
[27] M. Walther, D. G. Cooke, C. Sherstan, M. Hajar, M. R. Freeman, and F. A. Hegmann, Phys. Rev. B **76**, 125408 (2007).